# Wet-Spun Continuous Graphene Films

Zheng Liu,[†] Zheng Li,[†] Zhen Xu,[†] Zhixiang Xia,[‡] Xiaozhen Hu,[†] Liang Kou,[†] Li Peng,[†] Yangyang Wei,[†] and Chao Gao*,[†]

[†]MOE Key Laboratory of Macromolecular Synthesis and Functionalization, Department of Polymer Science and Engineering, and [‡]State Key Laboratory of Clean Energy Utilization, Institute for Thermal Power Engineering, Zhejiang University, 38 Zheda Road, Hangzhou 310027, P. R. China

Ⓢ Supporting Information

ABSTRACT: Macroscopic assembled, self-standing graphene and graphene oxide (GO) films have been demonstrated as promising materials in many emerging fields, such as Li ion battery electrodes, supercapacitors, heat spreaders, gas separation, and water desalination. Such films were mainly available on centimeter-scale via the time- and energy-consuming vacuum-filtration method, which seriously impedes their progress and large-scale applications. Due to the incompatibility between large-scale and ordered assembly structures, it remains a big challenge to access large-area assembled graphene thick films. Here, we report for the first time a fast wet-spinning assembly strategy to produce continuous GO and graphene thick films. A 20 m long, 5 cm wide, well-defined GO film was readily achieved at a speed of 1 m min^{-1}. The continuous, strong GO films were easily woven into bamboo-mat-like fabrics and scrolled into highly flexible continuous fibers. The reduced graphene films with high thermal and moderate electrical conductivities were directly used as fast-response deicing electrothermal mats. The fast yet controllable wet-spinning assembly approach paves the way for industrial-scale utilization of graphene.
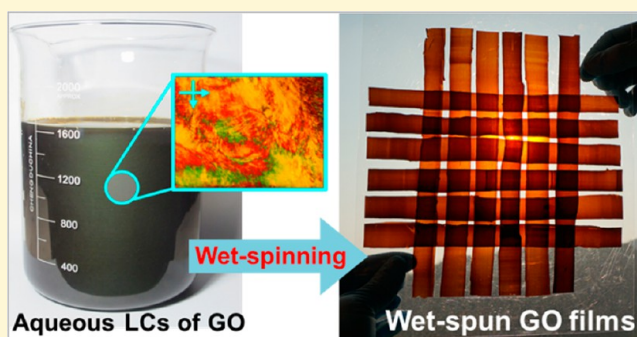
■ INTRODUCTION

Graphene, the first one-atom-thick, two-dimensional (2D) material, has been the focus of intensive research by virtue of its unique mechanical, electrical, and thermal attributes.[1−3] Large-area single- and few-layer graphene sheets are available by a high-temperature, roll-to-roll chemical vapor deposition (CVD) method,[4,5] opening the door to apply graphene in substrate-supported electronics and photonics. Alternatively, macroscopic assembled, free-standing graphene thick films/papers (GTFs) are accessible by room-temperature, solvent-based processing of graphene dispersions. GTFs are of crucial importance, since they have shown many promising applications that are not adept for CVD-made graphene thin films and their raw materials of powderlike graphene and graphene oxide (GO) are mass producible on an annual hundreds of tons scale by chemical exfoliation/oxidation of natural graphite. For instance, GTF-based supercapacitors performed high specific capacitance (>200 F g^{-1}) with excellent cycle stability.[6] When used as binder-free electrode materials for lithium batteries, GTFs possessed superb specific capacitance (864 mAh g^{-1}) with a Coulombic efficiency above 98% from the second cycle.[7] GTFs are also extremely useful in gas separation[8] and water desalination,[9,10] due to the precise and fast molecular sieving effect of their assembled layered structures.

The most classic approach to prepare GTFs is vacuum filtration of GO or chemically converted graphene (CCG),[11,12] enabling regularly packed layered structures. However, this method has insuperable problems of size limitation (centimeter scale) decided by the filtration apparatus and enormous consuming of time and energy due to the blocking effect of formerly packed layers to the more concentrated dispersions (e.g., a diameter of 5 cm and 10-μm-thick GO film commonly costs 2 days of continuous vacuum filtration, ~4 × 10^{-5} m^2 h^{-1}). Solution casting[13] and coating (dip, spray, spin, etc.)[14−17] were also attempted to prepare size-limited GO and CCG films. Recently, the electrospray deposition method has been used to prepare large-area graphene films,[18] and a relatively large graphene film was also archived by evaporation assembly.[19] All of these methods are lacking control over layered structures and uniform thickness in a large area. Due to the extremely difficult coordination between large-scale production and ordered assembly structures, well-defined GTFs cannot be accessed efficiently hitherto, hindering their practical applications. Accordingly, it calls for exploration of a scalable yet controllable assembly methodology to produce GTFs.[20]
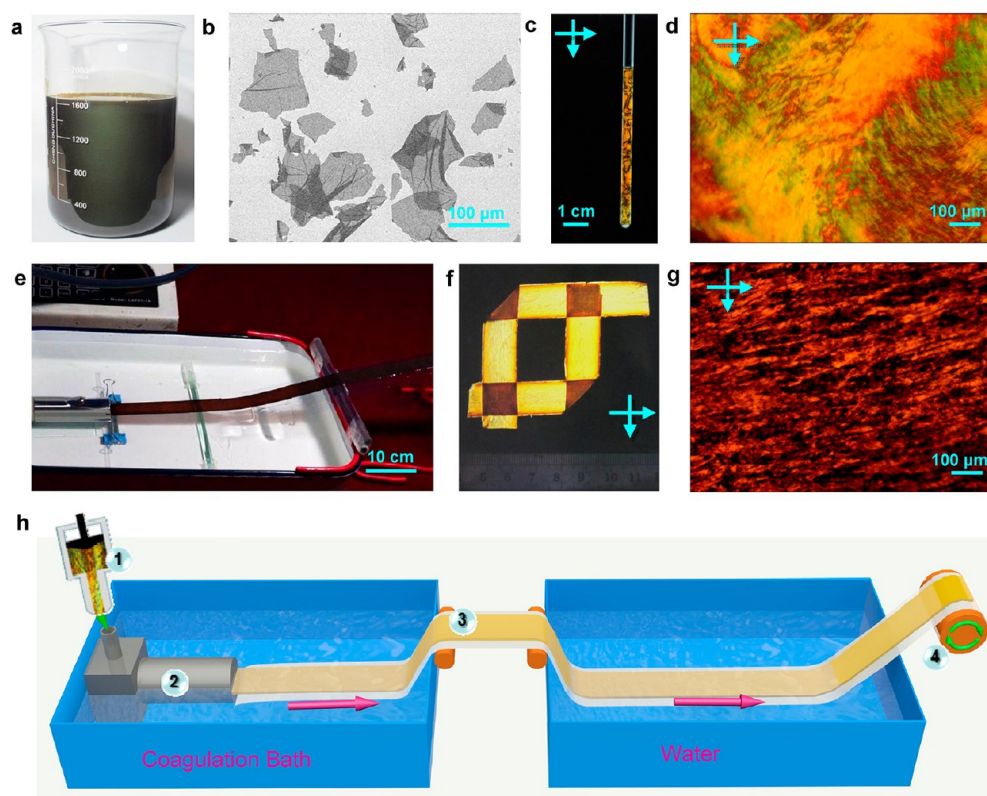
Here, inspired by the industrial melting process for continuous polymer films, we established for the first time a wet-spinning assembly methodology to produce quickly continuous GO films and GTFs. Through a thin and wide spinning channel, macroscopic assembled GO films (up to 20

Figure 1. (a) Homogeneous aqueous dispersion (1.6 L) of GO at a concentration of 10 mg mL^{-1}. (b) SEM image of GO sheets deposited on silicon. (c) Photograph of GO aqueous dispersion in a test tube between crossed polarizers, indicating its macroscopic LC feature. (d) POM image of GO LC loaded in a planar cell, at 10 mg mL^{-1}. (e) Photograph of wet-spinning of continuous GO film through a geometrically confined spinning channel. (f) Folded and overlapped GO gel films between crossed polarizers, indicating the highly oriented liquid crystalline domains. (g) POM image of GO gel films. (h) Schematic protocol for wet-spinning of continuous GO films: (1) the GO dispersion injector, (2) the spinning channel, (3) the coagulated GO gel film, and (4) the film wind-up reel.

m long and 15 cm wide) were continuously spun from the prealigned aqueous GO liquid crystals (LCs) at a fast speed up to 1 m min^{-1} in the presence of a coagulation bath. The continuous GO films with designed thickness (1.5−10 μm) and width (1−15 cm) possess highly ordered lamellar structures similar to the vacuum-filtered GO papers and thus show comparable or even superior mechanical strength. The flexible, self-standing GO films were readily woven into bamboo-mat-like fabrics and twisted into highly knittable scrolled fibers. After chemical reduction, the reduced continuous GTFs exhibited high thermal conductivity (530−810 W m^{-1} K^{-1}) and moderate electrical conductivity (12 000 S m^{-1}), promising as fast-response electrothermal materials for aircraft deicing. The wet-spinning assembly strategy was further extended to fabricate continuous nacre-mimetic composite films with fine "brick-and-mortar" structures by loading guests of nanoparticles or polymers into GO spinning dopes. Our methodology realized continuous processing of nanoparticles like polymers and opens the avenue to massive application of graphene.

RESULTS AND DISCUSSION

Large-Scale Preparation of GO LC Dope. Using the modified Hummers method,[21] we prepared GO sheets on a large-scale (250 g per batch) by expansion and oxidation of natural graphite (∼500 μm). Due to their abundant oxygen-containing functional groups, GO formed a stable, homogeneous dispersion in water (Figure 1a). The thickness of GO (t) was around 0.8 nm measured by atomic force microscopy

(AFM) [Figure S1h, Supporting Information (SI)], indicating its single-layer structure. The average lateral size (w) of the GO sheets was 21.9 μm with a distribution ranging from 3 to 50 μm and a polydispersity of 57.1% [Figures 1b and S1 (SI)]. The aqueous GO dispersion (10 mg mL^{-1}) displays macroscopic colorful textures in a test tube between crossed polarizers (Figure 1c) and shows typical Schlieren texture and vivid colors under polarized optical microscopy (POM), disclosing its nature of nematic LCs (Figure 1d).[22,23] The vivid birefringence is originated from oriented structures of local asymmetrical GO sheets with high aspect ratio ($w/t \approx 2.7 \times 10^4$). Such prealignment associated with GO LCs offers an ideal platform for the wet-spinning assembly of GO.

Continuous Wet-Spinning Assembly of GO Films. Wet-spinning technology has been widely employed for the industrial production of high-performance fibers from polymer LCs and solutions since 1891 (e.g., rayon, Nomex, and Kevlar). On the contrary, it was never been used to make polymer films because of the intrinsic contraction effect of a polymer solution during the coagulation/precipitation process, which makes it extremely difficult to control the morphology and ordered microstructures of polymer films in a large area. So, high-performance polymer films are solely produced by a melting process rather than the solution process of wet-spinning in industry.

GO and CCG can be recognized as indefinitely extended 2D aromatic macromolecules/polymers,[24] but they cannot be processed by the classic melting process methodology owing
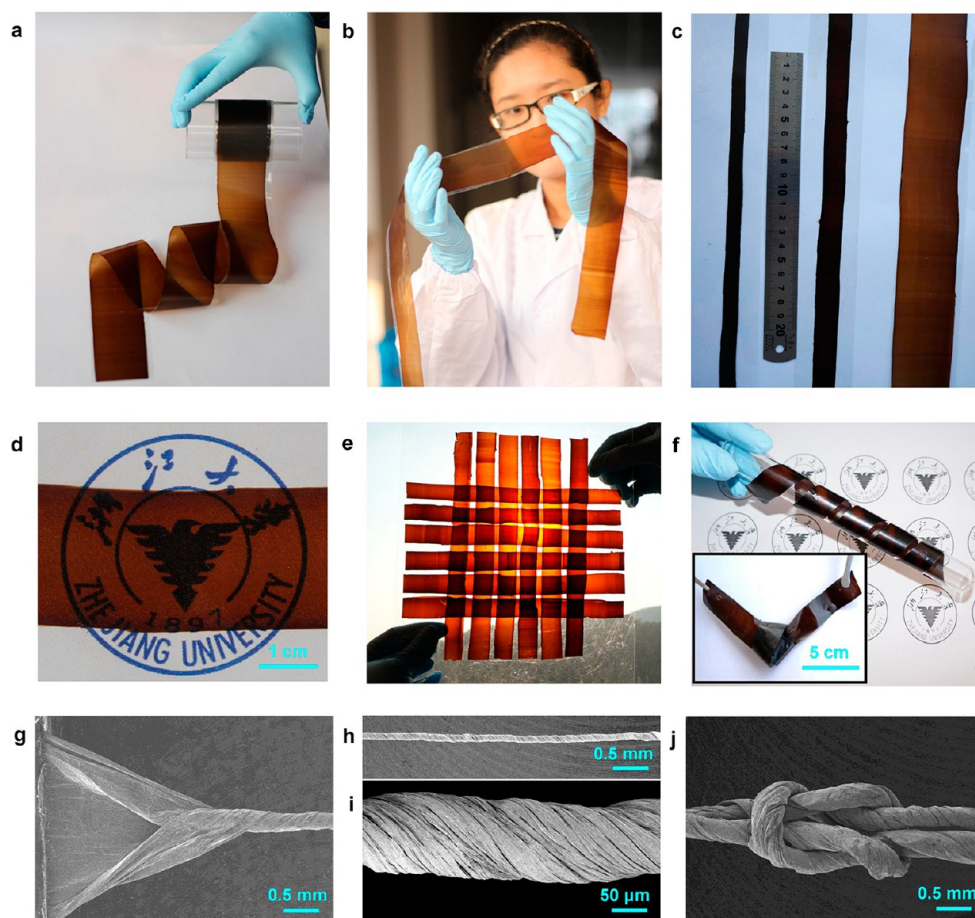
Figure 2. (a) A 20 m long and 5 cm width wet-spun GO film wound on a glass reel. (b) A hand-held semitransparent continuous GO film. (c) Continuous wet-spun GO films with designed widths of 1, 2, and 5 cm. (d) A semitransparent wet-spun GO film with thickness of 1.5 μm. (e) Hand-woven bamboo-mat-like fabric of wet-spun GO films. (f) Self-standing wet-spun GO film helically wrapped around a test tube and (inset) a knot of self-standing GO film. SEM images of (g) wet-spun GO film being twisted into a scrolled GO fiber, (h, i) surface morphology of scrolled GO fiber, and (j) Granny knot made by two scrolled fibers.

to the extremely high melting point of carbonaceous materials. Consequently, the solution processing methodology is the solely possible choice to access polymer-like continuous assembled graphene films. Questions arise: can we and how can we access continuous GTFs by the wet-processing approach?

Previously, our group found the lyotropic liquid crystallinity of GO in water and organic solvents[25−29] and first achieved continuous graphene fibers by wet-spinning of GO LCs following chemical reduction.[30−32] These findings, corroborated by following independent reports,[33−38] create versatile platforms to further explore more novel materials based on macroscopic assembly of graphene.

Herein, we try to achieve the first continuous GO and CCG films by wet-spinning of GO LCs using a specially designed spinning apparatus that contains a thin (0.200−1.0 mm) and wide (1−15 cm) spinning channel [Figures 1e,h and S2a (SI)]. The GO LC spinning dopes (10 mg mL^{-1}) were injected with a given speed from the spinning channel into the coagulation bath [ethanol/water (1:3 v/v) solutions of 5 wt % CaCl$_2$]. The fluid GO suspensions were transformed into gel films quickly (~10 s) with the aid of shear-flow-induced orientation and subsequent coagulation (Figure S2b, Video S1, SI). A continuous GO gel film with the length of 20 m was obtained within 20 min (with a speed of ~1 m min^{-1}). The as-prepared

GO gel films were simultaneously supported on a PET film. After water-washing and drying, the resulting wet-spun GO films were peeled off from the PET substrate to give self-standing wet-spun GO films. The productivity of our wet-spinning strategy is 60 m h^{-1} or 9 m^2 h^{-1} (or beyond if required), 5 orders of magnitude faster than the conventional vacuum-filtration method.

The GO gel films were placed between crossed polarizers to explore the evolution of GO LCs. As shown in Figure 1f, the oriented GO gel films show orientated golden yellow textures in comparison with the colorful textures of the original GO LC dope (Figure 1c). The transmittance of polarized light decreased dramatically in the vertically overlapped area (deep brown) due to the anisotropic polarization of oriented GO gel films. From the POM observation, the oriented GO gel films appear as large-scale fibriform LC textures along the flowing direction (Figure 1g). These results imply that the colloidal GO sheets were assembled into highly aligned GO LC domains parallel to the flowing direction under the shear flow stress of wet-spinning.

On the basis of our facile and scalable wet-spinning process, macroscopic assembled continuous wet-spun GO films up to 20 m long were achieved from the GO gel films after washing and drying (Figure 2a,b). Longer films, up to hundreds of meters, similar to the industrial polymer films, could be readily accessed
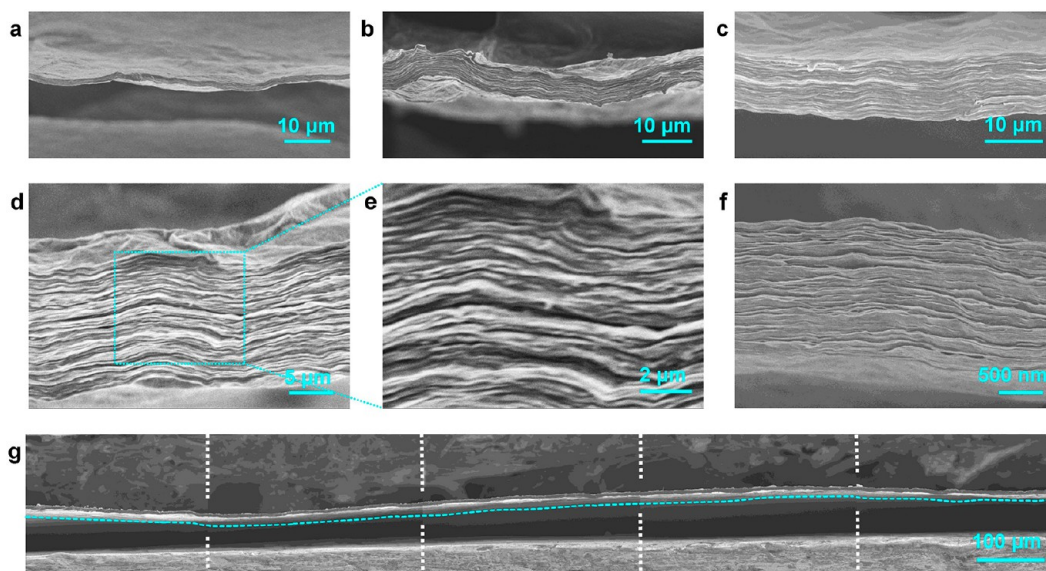
Figure 3. Cross sections of wet-spun GO films with thicknesses of (a) 1.5 μm, (b) 5.5 μm, and (c) 10.0 μm. (d, e) Section morphology of a wet-spun GO film, indicating highly ordered lamellar structures. (f) Cross section of a vacuum-filtration paper. (g) Continuous SEM images of wet-spun GO film, showing its uniform thickness.

by simple extension of the wet-spinning time. Meanwhile, it is convenient to control the thickness and width of GO films by modulating the size of the spinning channels. Accordingly, continuous GO films with widths of 1, 2, and 5 cm were successfully prepared (Figure 2c). We also got 15 cm wide GO films (adaptive for a flat panel computer like an iPad). Meter-wide continuous GO films suitable for industrial production are accessible through our wet-spinning assembly approach. The GO films are semitransparent (Figure 2b,d,e) and highly flexible (Figure 2d,e). The self-standing GO films are tough enough to be shaped on demand and are easily woven by hands into a large-area bamboo-mat-like fabric due to their broad width (Figure 2e). They are readily entangled on a test tube helically (Figure 2f), and a tight knot was tied without any breakage using the self-standing film (Figure 2f, inset).

Due to their flexibility, we twisted our continuous GO films into scrolled fibers using an electric motor.[39,40] As illustrated by a typical spinning wedge (Figure 2g), GO film converges to a scrolled fiber with uniform diameter possessing helical surface morphology (Figure 2h,i). Owing to their complex hierarchical structures, the scrolled fibers behave with higher flexibility and toughness and are easily tied into a granny knot (Figure 2j). Our scrolled fibers show an ultimate strain of 26% and tensile strength of 69 MPa (Figure S3, SI), which is comparable to that of scrolled carbon nanotube fibers (69−100 MPa).[41] This offers a facile approach to fabrication of continuous flexible graphene fibers from our continuous wet-spun films.

Ordered Microstructures of Wet-Spun GO Films. By adjusting the spinning channel, we obtained continuous GO films with various thicknesses ranging from 1.5 to 10 μm (Figure 3a−c). Thinner and thicker GO films are available by tuning either the concentration of the spinning dope or the thickness of the spinning channels. Despite the high thickness and fast wet-spinning process, the GO films showed highly ordered lamellar structures at the cross-section along the plane direction (Figure 3d,e), almost the same as the papers prepared by the slow vacuum-filtration protocol (Figure 3f). Figure 3g shows the SEM images of a 1.6 mm long cross section, and a continuous ordered layered structure with the same thickness

was observed throughout the entire cross section of the film. Such a uniform effect is ascribed to the homogeneous packing of oriented GO sheets at the direction perpendicular to the plane during the coagulation process. The flat morphology of the GO film surface with few fluctuations also confirms the formation of the stretched layered structures (Figure S5, SI).

Structural Evolution of Wet-Spun GO Films. The shear flow directing of GO sheets in the geometrically confined channel is the dominant mechanism that enables the anisotropic GO LCs to become final uniform structures. We traced the structural evolution of a GO LC dope during the wet-spinning process by the freeze-drying method. Figure 4 shows the corresponding SEM images and proposed structural evolution model. The continuous process to access a wet-spun film could be divided into three main stages of an arrowlike orientation (I), uniform alignment (II), and compact packing (III).

Before wet-spinning, the GO LC dope possesses prealigned liquid crystalline domains with dislocation. Under injection stress, stage I begins with the accordant orientation of anisotropic GO LCs in the spinning channel along the flowing direction. Both effects of the Newton's law of fluid viscosity and the resistance force of the spinning channel wall result in the formation of fluid layers with a velocity gradient (Figure 4a) (v/y, the rate of change of velocity (v) with the dimension (y) in the direction perpendicular to the plane). This makes the GO sheets orient with a vector (n) gradient. Consequently, the GO sheets evolve into an arrowlike orientating state (Figure 4b). From the channel wall to the center of the fluid ($y = 0$ to half of the channel height), the orientation angle (α) between the flowing axis and the plane of the GO sheets gradually decreases from around 45° to 0° (Figure 4b−d).

Stage II commences as the oriented GO dope is injected into the coagulation bath. Upon the exchange of solvent and coagulation bath, the spinning dope contracted mainly in the direction of thickness (perpendicular to the plane direction) into GO gel films quickly (in ~10 s). The thickness of the gel film becomes thinner and thinner, concentrating from 500 μm of the given channel thickness to around 125 μm. Due to the
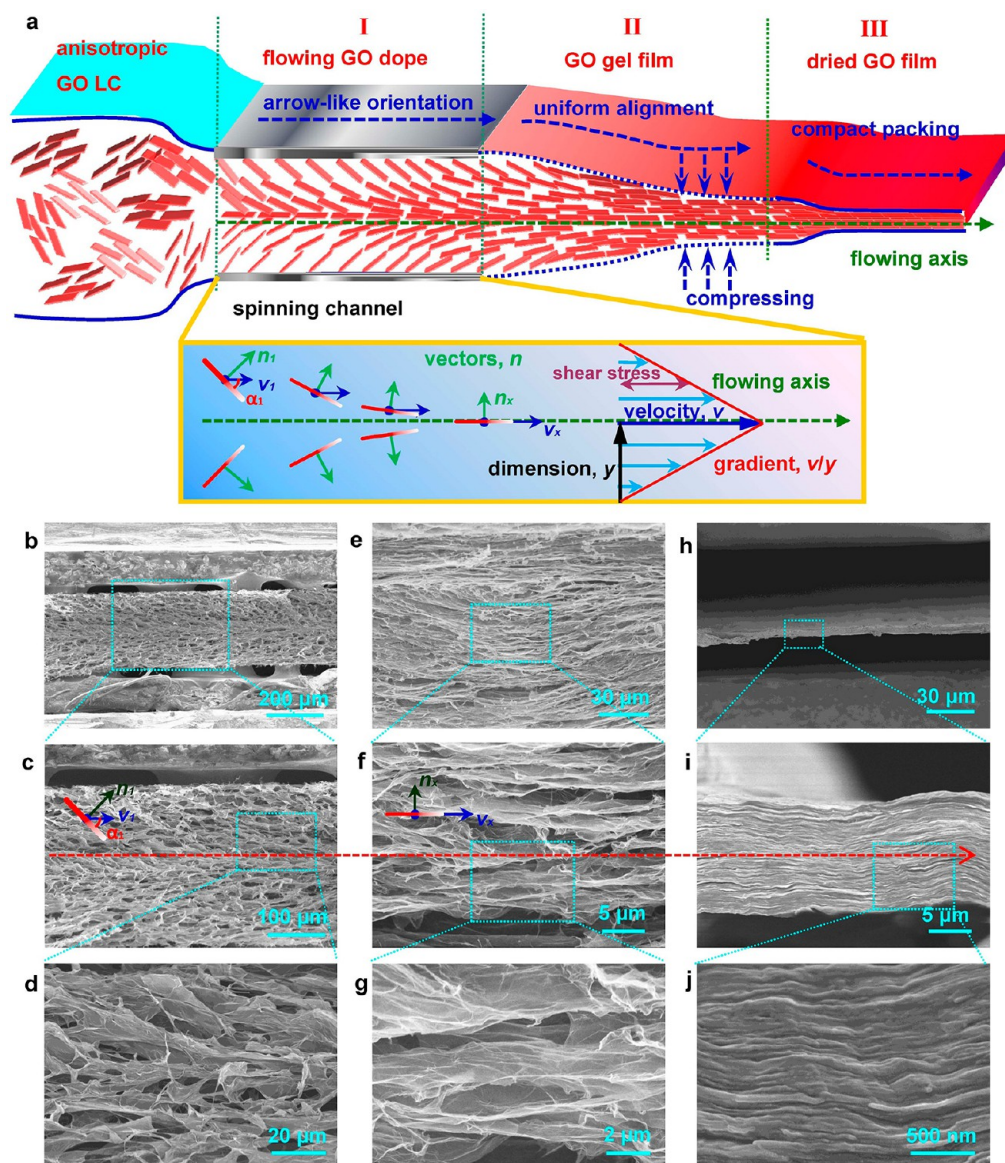
Figure 4. (a) Schematic diagram depicting the structural evolution with typical three stages: I, arrowlike orientation; II, uniform alignment; III, compact packing. Here, *n*, *v*, and α denote the orientation vector of GO, velocity of flowing layer, and the angle between GO sheets and flowing direction, respectively. Off-line cryo-SEM tracking of the wet-spinning process in the spinning channel (b−d), in the coagulation bath (e−g), and after drying (h−j).

vertically compressing force of coagulation, GO sheets then get uniformly aligned along the plane direction, and the orientation angle α of all GO sheets turns into nearly 0°. This aligned lamellar structure is confirmed by freeze-drying of the coagulated GO gel films (Figure 4e−g). Significantly, the contraction in the transverse direction of the gel film is nearly negligible. As observed from the cross-section of the gel film, the GO sheets are highly stretched with little surface wrinkles (Figure S6, SI). This effect makes the width of the wet-spun films precisely controlled and the defects/voids of films seldom generated, bringing long-range ordered structures.

Stage III denotes the solidifying/drying of gel films as they are taking out from the coagulation bath (Figure 4h−j). The interlayer spacing of GO sheets decreases continuously due to the gradual evaporation of solvents, leading to dramatic contraction of gel films in the direction perpendicular to the plane from 125 to ∼10 μm. Due to the strong self-assembly forces of van der Waals force, π−π stacking, and hydrogen

bonding, the aligned GO sheets tightly packed up to form continuous yet highly ordered films.

Properties of Wet-Spun GO and Graphene Films. Further analysis of X-ray diffraction (XRD) pattern shows that the continuous GO films exhibit a distinct peak at 2θ 9.81°, corresponding to the (001) interplanar spacing of 9.01 Å calculated from the 2θ value ($d = \lambda/2 \sin \theta$) (Figure 5a). This reveals that the layered GO films preserved the ordered lamellar structures from the oriented GO LCs. The *d*-spacing of continuous GO films is similar to that of vacuum-filtered GO papers (2θ = 10.13°, *d* = 8.72 Å). As calculated using the Debye−Scherrer equation ($D_{hkl} = k\lambda/\beta \cos \theta$), the sizes of the crystalline domains are 11.2 nm for continuous GO films and 15.7 nm for filtered GO papers, corresponding to about 12 and 18 stacked GO layers, respectively. When chemically reduced by aqueous hydriodic acid (HI, 40 wt %), the XRD pattern of the continuous reduced GO films, GTFs, presents a peak at 2θ = 24.62° corresponding to the (002) interplanar spacing of 3.61
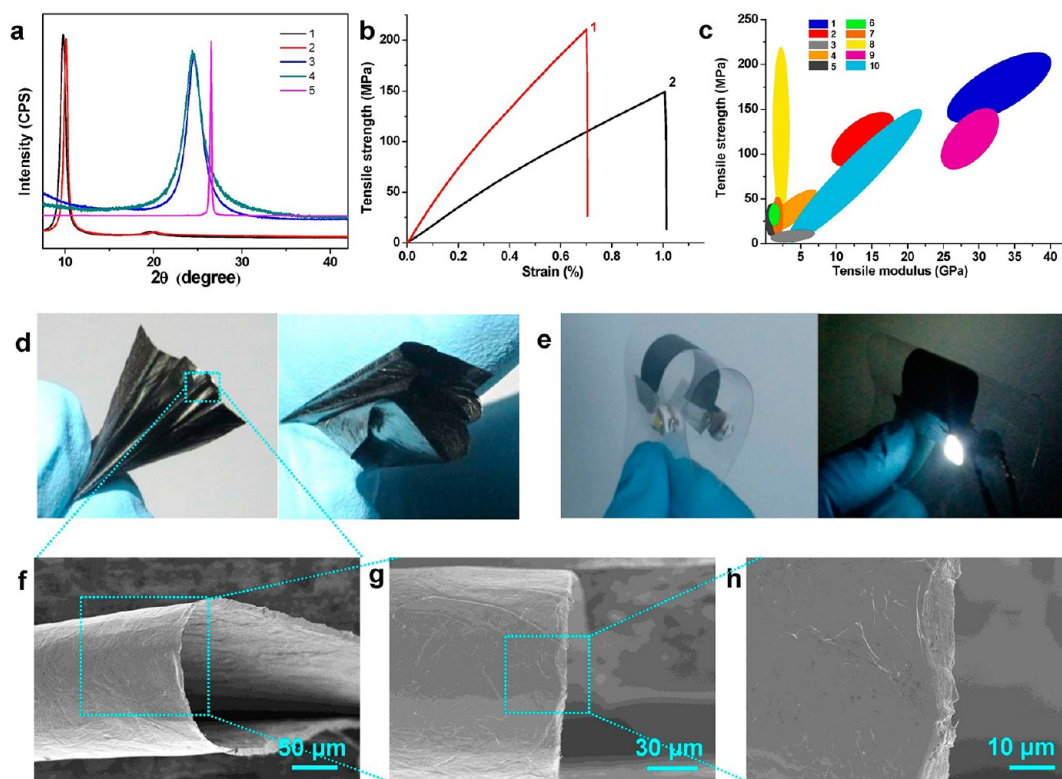
Figure 5. (a) XRD patterns of continuous wet-spun GO films and vacuum-filtered GO films before and after reduction: 1, wet-spun GO films; 2, filtered papers; 3, wet-spun graphene films; 4, filtered graphene papers; and 5, graphite. (b) Typical tensile−strain curves for continuous wet-spun GO films (1) and wet-spun graphene films (2). (c) The comparison of mechanical strength and modulus for carbonaceous and polymeric films: 1, wet-spun graphene films; 2, wet-spun GO films; 3, graphite foil; 4, carbon nanotube buckypaper; 5, HDPE; 6, PP; 7, PVC; 8, BOPP; 9, vacuum-filtered GO papers; 10, vacuum-filtered graphene papers (see Table S1, SI). (d) Extremely bent and sharply folded wet-spun graphene film showing no breakage. (e) Flexible and bendable conductor on PET substrate in the bent working state after 100 bending cycles. (f−h) SEM images of extremely bent wet-spun graphene film without any surface fractures.

Å (Figure 5a). The reduced filtered paper shows a peak at 2θ = 24.41° and d-spacing of 3.64 Å. The sizes of the crystalline domains are 5.29 nm for our continuous GTFs and 4.33 nm for the filtered graphene papers, corresponding to 15 and 12 stacked graphene layers, respectively. These results demonstrate that the ordered lamellar structure of continuous GO films is well-preserved after chemical reduction, and the wet-spun films hold comparable lamellar microstructures to the filtered papers.

Tensile tests of our wet-spun GO films revealed a tensile strength (σ) of 120.5 ± 28.9 MPa, Young's modulus (E) of 14.03 ± 2.76 GPa, and ultimate strain (ε) of 1.06 ± 0.36% (Figure 5b). As a comparison, we also prepared the filtered papers from the same batch of GO, which showed σ = 108.6 MPa and E = 11.6 GPa. This result suggests that our continuous wet-spun GO films are stronger than the vacuum-filtered GO films. In fact, the mechanical properties of our wet-spun GO films are generally superior to those of reported vacuum-filtered papers without additional cross-linking reinforcement (σ = 70−152 MPa)[20,42] and obviously stronger than those of evaporating-assembled (σ = 75.9 MPa)[43] and spray-coating (σ = 66 MPa)[18] films. The key reason is that the wet-spinning assembly favors the formation of long-range ordered structures with fewer defects because of the prealignment of GO LCs and in-plane shear stress in geometrically confined channel. Other methods like filtration and coating lack such effects, resulting in poor control over the film structures in a large area and thus more defects and weaker strength.

After reduction, the continuous wet-spun GFTs showed even stronger mechanical properties, which are σ = 172.2 ± 38.1 MPa, E = 32.36 ± 6.76 GPa, and ε = 0.71 ± 0.12%. Furthermore, the reduced films are also highly flexible, not breaking even after being extremely bent or sharply folded [Figures 5d,f−h and S7 (SI)].

Moreover, our reduced continuous GFTs without thermal treatment exhibit high lateral thermal conductivity (530−810 W m^{-1} K^{-1}) and good electrical conductivity [(1.2−2.1) × 10^4 S m^{-1}] due to their long-range, highly ordered microstructures. Further thermal annealing could dramatically improve their thermal (>1200 W m^{-1} K^{-1}) and electrical (>10^5 S m^{-1}) conductivities,[18,19,37] which will be reported elsewhere. Depending on their high conductivity and flexibility, our continuous graphene films are promising for wearable electronics. A bendable circuit was constructed with the graphene films as main conductor (Figure 5e), and it kept working after bending to 180°, as indicated by the lightening of LED chips. After 100 cycles of bending and relaxation, the circuit was still working and flexible. These multifunctional features offer continuous graphene films many practical applications beyond those of conventional polymer films.

Wet-Spun Graphene Films for Electrothermal Application and Deicing. The high thermal and moderate electrical conductivities of our GTFs make them an ideal candidate for use as a fast-response electrothermal material for a heat patch.[44−46] We made a bendable electrothermal patch by fixing a reduced graphene film (2 × 5 cm^2) on a polyimide

6791

dx.doi.org/10.1021/cm5033089 | *Chem. Mater.* 2014, 26, 6786−6795
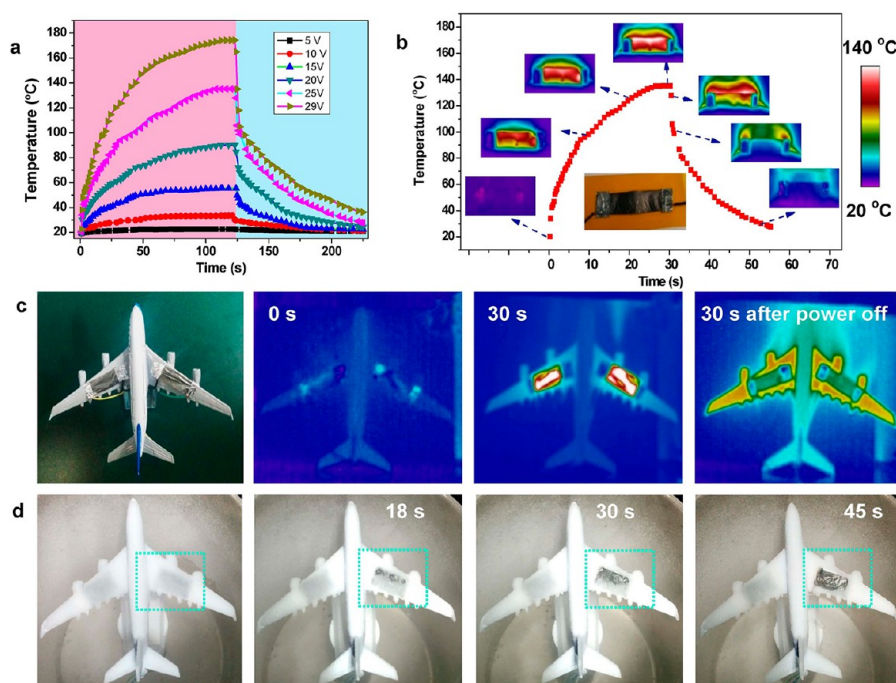
Figure 6. (a) Temperature profiles of a wet-spun graphene film heater under different applied dc voltages. (b) Real time infrared thermal images of a wet-spun graphene film heater applying a safe input voltage of 25 V. The temperature distribution was measured continuously by an infrared thermal imager. (c) Real time infrared thermography of a wet-spun graphene film heater applying a safe input voltage of 25 V on A380 plane model. (d) Ultrafast deicing process of a wet-spun graphene film heater on A380 plane model at −70 °C in a tank.

substrate (Figure 6). Voltages were applied on the graphene film heater using a direct current power supplier and the temperature was monitored by a portable infrared thermometer. Figure 6a shows the temperature profiles of the graphene film heater under different applied dc voltages. The temperature of the graphene heat patch increased rapidly in the initial 25−30 s (e.g., from 20 to 122 °C for the case of 29 V, ~4 °C s^{-1}), gradually in the following 50−60 s, and then approached to a steady-state at around 2 min. The temperature rose to 33, 54, 90, 138, and 177 °C within 2 min at input safe voltages of 10, 15, 20, 25, and 29 V, respectively. The corresponding power consumptions and convective heat-transfer coefficients based on two sides of our wet-spun graphene films are listed in Table S1 (SI), indicating the linear relationship between input power and steady-state temperature (Figure S8, SI). When the applied voltage was removed, the temperature decreased sharply, especially for the cases of high voltages (e.g., drop from 177 to 138 °C in 1 s for the case of 29 V), due to the high thermal conductivity of graphene films.

Such a fast-response electrothermal effect was confirmed using a real time infrared thermal imager (Figure 6b). Similarly, the temperature steeply rose from 20 to 130 °C in 25 s (a heating rate of 5.2 °C s^{-1}) and remained at 138 °C after 30 s in the case of 25 V. The fast-response graphene electrothermal patch performed homogeneous temperature distribution with continuous heat dissipation to the substrate.

Because of their integrated advantages of a fast electro-thermal Joule effect, light weight (density ~1.5 g cm^{-3}), high flexibility, and scalable productivity, the wet-spun graphene films are highly useful in many practical fields. Given that many aircraft accidents were related to icing of planes at either high altitude or apron since a piece of ice as thin as sandpaper on an aircraft wing can reduce wing lift by ~30% and increase drag by ~40%, ultrafast and safe deicing is of extreme importance for aircrafts. Nichrome is one of the most used resistive materials in electrothermal appliances, but this alloy suffers from brittleness, high density (>8 g cm^3), and small resistivity (~10^{-6} Ω m).[46] To resolve such a problem, here we use our wet-spun graphene film heaters for ultrafast deicing on an A380 plane model. As shown in Figure 6c, the graphene film patches covering the wings get to 105 °C within only 5 s (21 °C s^{-1}) and reach its steady-state temperature of 138 °C in 30 s under an applied safe voltage of 25 V. This verifies the ultrafast heating effect of the wet-spun graphene films attached on plane wings. Notably, plane wings remained at 50−60 °C when the graphene patch was cooled to room temperature in 30 s, indicating the high thermal conductivity of our graphene films.

The fast electrothermal effect and heat spreading enables a cubic bulk of ice (1 × 2 × 1 cm^3) to melt completely in 50 s (Figure S8, SI). To mimic the low-temperature condition at the stratosphere (around −50 °C), we put the plane model into a −70 °C tank. As shown in Figure 6d, the whole model plane was iced up with a 0.6 cm-thick ice layer by spraying water. After being heated for only 10 s with a safe voltage of 25 V, the melting of ice was observed (note: only the right wing was heated for comparison), and the layer of ice covering the heater film completely melted and flowed away from the area of the graphene patch in 45 s (Video S2, SI). In addition, no ice froze on the heating patch under further water spraying when the electrical power was kept on. These results open the door for our wet-spun graphene films to be applied in deicing of aircrafts and radars, as well as when other electrothermal effects are needed.

Macroscopic polymer films are all around us and have played a major part in our daily lives for more than half a century (e.g., plastic bags, packages, bottles, and films). Nevertheless, such polymer films are only accessible by a melting process. Due to
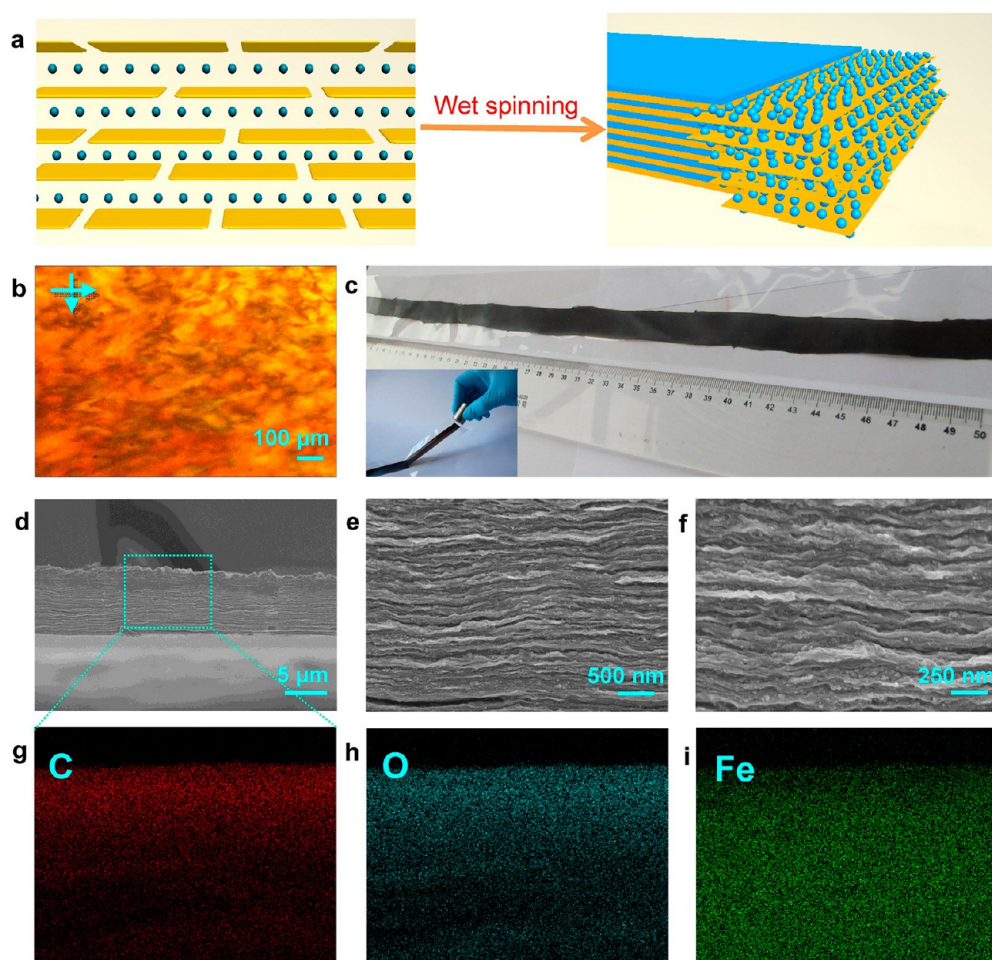
Figure 7. (a) Schematic protocol for the wet-spinning of continuous GO-based composites films via a liquid crystal self-templating mechanism. (b) POM image of GO/Fe$_3$O$_4$ mixture suspension, showing vivid liquid crystalline Schlieren textures. (c) A 1 m long, 2.5 cm wide nacre-mimetic GO-Fe$_3$O$_4$ NPs film. Inset: the composite film moving by the action of an external magnet. (d−f) SEM images of the GO−Fe$_3$O$_4$ NPs film section morphology, demonstrating highly ordered lamellar structures. EDS mapping images of carbon (g), oxygen (h), and Fe (i) elements of the GO−Fe$_3$O$_4$ NPs film section.

the isotropic contraction of polymer solutions, wet-spun continuous polymer films have never been reported yet.

Considering GO as unique 2D aromatic macromolecules,[47] we successfully accessed the first continuous GO films by an industrially viable wet-spinning methodology. In our opinion, the large sheet size with high aspect ratio ($w/t \approx 2.7 \times 10^4$) of GO LC phases enables the long-range macroscopic orientation and large-scale assembly of 2D films. The 2D GO sheets with high in-plane modulus, large lateral size, and relatively small interlayer spacing bring an efficient space restriction that holds on their fluid alignment and stretching state during the process of coagulation and solidifying (Figure 4). This unique effect makes the contraction of GO gel films limited to the vertical direction, and the width of the dried films is almost kept invariant to the gel films. Accordingly, despite an extremely diluted spinning concentration (∼1 wt %) and ultrahigh contraction ratio at the thickness direction (98%), the resulting GO films still retained highly aligned microstructures and long-range ordered macrostructures, and hence, they showed superior mechanical performance. After reduction, the continuous graphene films inherited the lamellar ordering that provides excellent mechanical property and high thermal and electrical conductivities.

Figure 5c lists the comparison of mechanical strength and modulus for carbonaceous and polymeric films. The continuous wet-spun graphene films are much stronger than the commercial hot-pressing graphite foil/papers ($\sigma \sim 5$ MPa),[48] carbon nanotube buckypapers ($\sigma = 10-74$ MPa),[49] and most of polymer films ($\sigma_s = 20-70$ MPa). Compared with the classic linear polymer films of HDPE (high density polyethylene, $\sigma = 17-45$ MPa), PP (polypropylene, $\sigma = 31-43$ MPa), PVC (polyvinyl chloride, $\sigma = 10-55$ MPa), and PET (polyethylene terephthalate, $\sigma = 8-55$ MPa), our films of 2D graphene macromolecules displayed 3−25 times higher strength. The highest strength of our solution-processed graphene films (210 MPa) is even comparable to those of BOPP films (biaxial-oriented PP, $\sigma = 120-240$ MPa). In addition, our wet-spun graphene films are 3−4 times stiffer than the carbonaceous ($E = 0.8-5$ GPa) and polymeric films ($E = 0.6-4.1$ GPa). This creates an unprecedented wet-spinning assembly strategy to prepare quickly and continuously high-performance, multifunctional nonmetallic material films.

It is known that the vacuum-filtration method can be applied to prepare graphene-polymer composite films/papers with nacre-mimetic "brick-and-mortar" (B&M) microstructures.[50] However, despite mimicking for more than 20 years, no solution has been established to access continuous nacre-

mimetic films, hindering the scalable application of such ideally structured biomimic materials.[51,52] Here, we extend our wet-spinning assembly strategy to resolve such a big challenge. By direct wet-spinning of the mixture of GO LC and poly(vinyl alcohol) (PVA), we achieved continuous GO−PVA composite films with PVA content of 33 wt % via a liquid crystal self-templating mechanism,[53] which showed fine B&M structures and a nacre-exceeding high mechanical performance of $\sigma = 266$ MPa (Figure S10, SI), higher than graphene-polymer nacre-mimetic papers made by vacuum-filtration method ($\sigma = 150-230$ MPa).[54]

Moreover, this strategy is extended to make continuous, multifunctional composite films of all inorganic particles (Figure 7b), by wet-spinning a mixture of GO LC and Fe_3O_4 nanoparticles (NPs). Because of the superparamagnetism of Fe_3O_4 NPs,[55] the GO/Fe_3O_4 hybrid film moves regularly under the action of an external magnet (inset of Figure 7c and Video S3, SI). SEM observations on the film cross-section reveal a highly ordered lamellar morphology (Figure 7d), and well-dispersed Fe_3O_4 NPs are clearly found from the highly magnified SEM images (Figure 7e,f). The energy-dispersive spectroscopy (EDS) mapping confirms the homogeneous distributions of C, O, and Fe elements [Figures 7g−i and S9 (SI)]. This opens an avenue to continuous graphene-based composite films with tailor-made and integrated properties.

CONCLUSIONS

In conclusion, we established for the first time a facile, general yet controllable wet-spinning assembly methodology to prepare continuous, thick films of neat GO and graphene. The films with homogeneous thickness were produced in a high speed (1 m min^{-1} and beyond). Through cryo-technology, we traced the whole wet-spinning process and proposed a model for the formation of continuous GO films. The combination of shear-induced uniform alignment of LC spinning dope and negligible in-plane contraction of coagulated GO sheets resulted in long-range highly ordered lamellar structures of continuous, width-designed films. The as-made continuous GO films are flexible and tough enough to be woven into large-area bamboo-mat-like fabrics and scrolled into highly flexible continuous fibers. The fast available GO and graphene films showed superior mechanical properties to their analogous time- and energy-consuming vacuum-filtered papers. The chemically reduced GO films with high thermal and moderate electrical conductivities were demonstrated as desirable materials for fast-response electrothermal patches for deicing and other applications. This versatile wet-spinning assembly strategy was extended to fabricate the first continuous, multifunctional nacre-mimetic composite films via a liquid crystal self-templating mechanism. The realization of continuous graphene films breaks new ground for macroscopic practical applications of graphene, the wonder 2D nanoparticle.

EXPERIMENTAL SECTION

Wet-Spinning of Continuous GO and GO-Based Nacre-Mimetic Composite Films. The continuous GO films were made by the wet-spinning assembly approach as depicted in Figure 1h. Typically, GO suspensions (10.0 mg mL^{-1}) were injected into the coagulation bath at a spinning rate of 12 mL min^{-1} (about 1 m min^{-1}) using a thin and wide spinning channel with a rectangular cross section. The coagulation bath is an ethanol/water (1:3 v/v) solution with 5 wt % CaCl$_2$. The GO gel films were coagulated, simultaneously supported on a PET film, and transferred into a water bath to wash away the residual coagulation solution. The wet gel films were dried at

40 °C in air for 2 h and then dried at 60 °C under vacuum for 4 h. The supported GO films were then immersed in water for 2 h, detached from the PET films, and dried at 60 °C under vacuum for 12 h to give the final self-standing wet-spun GO films.

The GO/Fe_3O_4 mixed solution was prepared by adding 25 wt % Fe_3O_4 aqueous solution into GO aqueous solution dropwise with mechanical stirring. The initial Fe_3O_4 nanoparticles were characterized by dynamic laser light scattering and SEM (Figure S9,SI). The GO/PVA composite was prepared by adding 0.06 g mL^{-1} PVA solution into GO aqueous solution with magnetic stirring. Then, the GO/Fe_3O_4 and GO/PVA composite films were spun from corresponding spinning dopes using the same protocol as the case of neat GO films.

Chemical Reduction of GO Films.[56−58] Dried GO films were helically wrapped on a test tube, as shown in Figure 2f, immersed into the HI solution (40%), and kept at 80 °C for 12 h. Subsequently, the films were rinsed with a saturated sodium bicarbonate solution, water, and ethanol and dried at 100 °C under vacuum for 12 h.

Instrumentation. Scanning electron microscopy (SEM) images were collected on a Hitachi S4800 field emission SEM system. Atomic force microscopy (AFM) characterization was performed on a NSKSPI3800 under tapping mode with samples prepared by spin-coating onto freshly peeled mica substrates at 1200 rpm from diluted sample solutions. The X-ray diffraction (XRD) measurements were taken on a Philips X'Pert PRO diffractometer equipped with Cu KR radiation (40 kV, 40 mA) with an X-ray wavelength (λ) of 1.5418 Å. Polarized optical microscopy (POM) observations were performed using a Nikon E600POL. The tensile tests were carried out on an HS-3002C mechanical testing system. GO and graphene films were cut to 3-mm-wide films. Both ends of the individual film were fixed onto clamps made by two PDMS slices with gauge lengths of 10 mm, respectively. A loading rate of 2 mm min^{-1} was applied in all mechanical tests. The cross-section area was determined from SEM images of the fracture section. The Young's modulus was calculated from the initial, linear regime of stress−strain curves. For each type of films, at least 15 samples were tested. Lateral thermal diffusivity was measured by a Netzsch LFA 457 laser flash thermal diffusivity apparatus operated at room temperature. Thermal conductivity of the reduced wet-spun graphene films was determined according to ref 59. A dc power supply (APS3005Dm, Atten) was used to apply an electrical potential across GTFs for the heater tests. The surface temperature of the films was recorded using a portable infrared thermometer (Smart Sensor AR350+) during the electrothermal measurements. Infrared thermography was taken using a FLIR ThermaCAM S65 system.

ASSOCIATED CONTENT

S Supporting Information

Figures S1−S10, Tables S1 and S2, and Videos S1−S3, showing supporting results from additional experiments. This material is available free of charge via the Internet at http://pubs.acs.org.

AUTHOR INFORMATION

Corresponding Author

*E-mail: chaogao@zju.edu.cn.

Author Contributions

C.G. conceived the concept; Z. Liu and C.G. designed the research, analyzed the experimental data, and wrote the paper; Z. Li, Z. Xu, Z. Xia, X.H., L.K., L.P., and Y.W. contributed to some experiments and took part in discussions; and C.G. supervised and directed the project. All authors have given approval to the final version of the manuscript.

Notes

■ REFERENCES

(1) Geim, A. K.; Novoselov, K. S. Nat. Mater. 2007, 6, 183−191.
(2) Novoselov, K. S.; Falko, V. I.; Colombo, L.; Gellert, P. R.; Schwab, M. G.; Kim, K. Nature 2012, 490, 192−200.
(3) Ruoff, R. Nature 2012, 483, S42−S42.
(4) Kim, K. S.; Zhao, Y.; Jang, H.; Lee, S. Y.; Kim, J. M.; Kim, K. S.; Ahn, J.-H.; Kim, P.; Choi, J.-Y.; Hong, B. H. Nature 2009, 457, 706−710.
(5) Bae, S.; Kim, H.; Lee, Y.; Xu, X. F.; Park, J. S.; Zheng, Y.; Balakrishnan, J.; Lei, T.; Kim, H. R.; Song, Y. I.; Kim, Y. J.; Kim, K. S.; Ozyilmaz, B.; Ahn, J. H.; Hong, B. H.; Iijima, S. Nat. Nanotechnol. 2010, 5, 574−578.
(6) Yang, X.; Zhu, J.; Qiu, L.; Li, D. Adv. Mater. 2011, 23, 2833−2838.
(7) Liu, F.; Song, S.; Xue, D.; Zhang, H. Adv. Mater. 2012, 24, 1089−1094.
(8) Kim, H. W.; Yoon, H. W.; Yoon, S. M.; Yoo, B. M.; Ahn, B. K.; Cho, Y. H.; Shin, H. J.; Yang, H.; Paik, U.; Kwon, S.; Choi, J. Y.; Park, H. B. Science 2013, 342, 91−95.
(9) Han, Y.; Xu, Z.; Gao, C. Adv. Funct. Mater. 2013, 23, 3693−3700.
(10) Koenig, S. P.; Wang, L. D.; Pellegrino, J.; Bunch, J. S. Nat. Nanotechnol. 2012, 7, 728−732.
(11) Dikin, D. A.; Stankovich, S.; Zimney, E. J.; Piner, R. D.; Dommett, G. H. B.; Evmenenko, G.; Nguyen, S. T.; Ruoff, R. S. Nature 2007, 448, 457−460.
(12) Li, D.; Muller, M. B.; Gilje, S.; Kaner, R. B.; Wallace, G. G. Nat. Nanotechnol. 2008, 3, 101−105.
(13) Zhou, S.; Zhu, Y.; Du, H.; Li, B.; Kang, F. New Carbon Mater. 2012, 27, 241−249.
(14) Kim, H. M.; Lee, J. K.; Lee, H. S. Thin Solid Films 2011, 519, 7766−7771.
(15) Becerril, H. A.; Mao, J.; Liu, Z.; Stoltenberg, R. M.; Bao, Z.; Chen, Y. ACS Nano 2008, 2, 463−470.
(16) Pham, V. H.; Cuong, T. V.; Hur, S. H.; Shin, E. W.; Kim, J. S.; Chung, J. S.; Kim, E. J. Carbon 2010, 48, 1945−1951.
(17) Kim, D. Y.; Sinha Ray, S.; Park, J. J.; Lee, J. G.; Cha, Y. H.; Bae, S. H.; Ahn, J. H.; Jung, Y. C.; Kim, S. M.; Yarin, A. L.; Yoon, S. S. Adv. Funct. Mater. 2014, 24, 4986−4995.
(18) Xin, G.; Sun, H.; Hu, T.; Fard, H. R.; Sun, X.; Koratkar, N.; Borca-Tasciuc, T.; Lian, J. Adv. Mater. 2014, 26, 4521−4526.
(19) Shen, B.; Zhai, W.; Zheng, W. Adv. Funct. Mater. 2014, 24, 4542−4548.
(20) Compton, O. C.; Nguyen, S. T. Small 2010, 6, 711−723.
(21) Xu, Z.; Sun, H.; Zhao, X.; Gao, C. Adv. Mater. 2013, 25, 188−193.
(22) Aboutalebi, S. H.; Gudarzi, M. M.; Zheng, Q. B.; Kim, J. K. Adv. Funct. Mater. 2011, 21, 2978−2988.
(23) Shen, T. Z.; Hong, S. H.; Song, J. K. Nat. Mater. 2014, 13, 394−399.
(24) Chen, D.; Tang, L.; Li, J. Chem. Soc. Rev. 2010, 39, 3157−3180.
(25) Xu, Z.; Gao, C. Acc. Chem. Res. 2014, 47, 1267−1276.
(26) Xu, Z.; Gao, C. ACS Nano 2011, 5, 2908−2915.
(27) Sun, H.; Xu, Z.; Gao, C. Adv. Mater. 2013, 25, 2554−2560.
(28) Liu, Z.; Xu, Z.; Hu, X.; Gao, C. Macromolecules 2013, 46, 6931−6941.
(29) Zhao, X.; Xu, Z.; Xie, Y.; Zheng, B.; Kou, L.; Gao, C. Langmuir 2014, 30, 3715−3722.
(30) Xu, Z.; Gao, C. Nat. Commun. 2011, 2, 571.
(31) Xu, Z.; Zhang, Y.; Li, P.; Gao, C. ACS Nano 2012, 6, 7103−7113.
(32) Xu, Z.; Liu, Z.; Sun, H.; Gao, C. Adv. Mater. 2013, 25, 3249−3253.
(33) Aboutalebi, S. H.; Jalili, R.; Esrafilzadeh, D.; Salari, M.; Gholamvand, Z.; Aminorroaya Yamini, S.; Konstantinov, K.; Shepherd, R. L.; Chen, J.; Moulton, S. E.; Innis, P. C.; Minett, A. I.; Razal, J. M.; Wallace, G. G. ACS Nano 2014, 8, 2456−2466.
(34) Cong, H.; Ren, X.; Wang, P.; Yu, S. Sci. Rep. 2012, 2, 613.
(35) Xiang, C.; Young, C. C.; Wang, X.; Yan, Z.; Hwang, C.-C.; Cerioti, G.; Lin, J.; Kono, J.; Pasquali, M.; Tour, J. M. Adv. Mater. 2013, 25, 4592−4597.
(36) Dong, Z.; Jiang, C.; Cheng, H.; Zhao, Y.; Shi, G.; Jiang, L.; Qu, L. Adv. Mater. 2012, 24, 1856−1861.
(37) Jalili, R.; Aboutalebi, S. H.; Esrafilzadeh, D.; Shepherd, R. L.; Chen, J.; Aminorroaya-Yamini, S.; Konstantinov, K.; Minett, A. I.; Razal, J. M.; Wallace, G. G. Adv. Funct. Mater. 2013, 23, 5345−5354.
(38) Wu, D. Q.; Zhang, F.; Liang, H.; Feng, X. Chem. Soc. Rev. 2012, 41, 6160−6177.
(39) Cheng, H.; Hu, Y.; Zhao, F.; Dong, Z.; Wang, Y.; Chen, N.; Zhang, Z.; Qu, L. Adv. Mater. 2014, 26, 2909−2913.
(40) Cruz-Silva, R.; Morelos-Gomez, A.; Kim, H.-i.; Jang, H.-k.; Tristan, F.; Vega-Diaz, S.; Rajukumar, L. P.; Elias, A. L.; Perea-Lopez, N.; Suhr, J.; Endo, M.; Terrones, M. ACS Nano 2014, 8, 5959−5967.
(41) Li, Y.; Shang, Y.; He, X.; Peng, Q.; Du, S.; Shi, E.; Wu, S.; Li, Z.; Li, P.; Cao, A. ACS Nano 2013, 7, 8128−8135.
(42) Park, S.; Lee, K.-S.; Bozoklu, G.; Cai, W.; Nguyen, S. T.; Ruoff, R. S. ACS Nano 2008, 2, 572−578.
(43) Chen, C. M.; Yang, Q. H.; Yang, Y.; Lv, W.; Wen, Y.; Hou, P. X.; Wang, M.; Cheng, H. M. Adv. Mater. 2009, 21, 3007−3011.
(44) Janas, D.; Koziol, K. Nanoscale 2014, 6, 3037−3045.
(45) Sui, D.; Huang, Y.; Huang, L.; Liang, J.; Ma, Y.; Chen, Y. Small 2011, 7, 3186−3192.
(46) Janas, D.; Koziol, K. K. Carbon 2013, 59, 457−463.
(47) Weng, Z.; Xu, Z.; Gao, C. Sci. China Chem. 2014, 57, 605−614.
(48) Dowell, M. B.; Howard, R. A. Carbon 1986, 24, 311−323.
(49) Zhang, X.; Sreekumar, T. V.; Liu, T.; Kumar, S. J. Phys. Chem. B 2004, 108, 16435−16440.
(50) Yao, H.; Fang, H.; Wang, X.; Yu, S. Chem. Soc. Rev. 2011, 40, 3764−3785.
(51) Hu, X.; Xu, Z.; Gao, C. Sci. Rep. 2012, 2, 767.
(52) Kou, L.; Gao, C. Nanoscale 2013, 5, 4370−4378.
(53) Hu, X.; Xu, Z.; Liu, Z.; Gao, C. Sci. Rep. 2013, 3, 2374.
(54) Huang, L.; Li, C.; Yuan, W.; Shi, G. Nanoscale 2013, 5, 3780−3786.
(55) Gao, C.; Li, W. W.; Morimoto, H.; Nagaoka, Y. J. Phys. Chem. B 2006, 14, 7213−7220.
(56) Kou, L.; Huang, T.; Zheng, B.; Han, Y.; Zhao, X.; Gopalsamy, K.; Sun, H.; Gao, C. Nat. Commun. 2014, 5, 3754.
(57) Huang, T.; Zheng, B.; Kou, L.; Gopalsamy, K.; Xu, Z.; Gao, C.; Meng, Y.; Wei, Z. RSC Adv. 2013, 3, 23957−23962.
(58) Pei, S.; Zhao, J.; Du, J.; Ren, W.; Cheng, H. M. Carbon 2010, 48, 4466−4474.
(59) Kong, Q. Q.; Liu, Z.; Gao, J. G.; Chen, C. M.; Zhang, Q.; Zhou, G.; Tao, Z. C.; Zhang, X. H.; Wang, M. Z.; Li, F.; Cai, R. Adv. Funct. Mater. 2014, 24, 4222−4228.